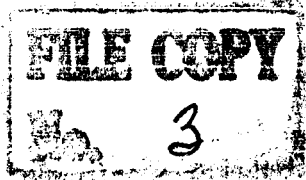


UNCLASSIFIED

Copy 50

NASA TM X-14

NASA TM - X-14



# TECHNICAL MEMORANDUM

## X-14

AN INVESTIGATION OF AN UNDERSLUNG NOSE INLET WITH VARIOUS  
NOSE CONFIGURATIONS AT MACH NUMBERS

FROM 1.55 TO 2.23

By Norman E. Sorensen and Rex R. Ellington

Ames Research Center  
Moffett Field, Calif.

CLASSIFICATION CHANGED TO UNCLASSIFIED  
BY AUTHORITY OF NASA PUB. ANN. NO. 211  
DATE 10/23/70  
*jm*

NASA LIBRARY  
AMES RESEARCH CENTER  
MOFFETT FIELD, CALIF.

CLASSIFIED DOCUMENT - TITLE UNCLASSIFIED

This material contains information affecting the national defense of the United States within the meaning of the espionage laws, Title 18, U.S.C., Secs. 793 and 794, the transmission or revelation of which in any manner to an unauthorized person is prohibited by law.

NATIONAL AERONAUTICS AND SPACE ADMINISTRATION

WASHINGTON

August 1959

UNCLASSIFIED

8886

UNCLASSIFIED

[REDACTED]

## NATIONAL AERONAUTICS AND SPACE ADMINISTRATION

## TECHNICAL MEMORANDUM X-14

AN INVESTIGATION OF AN UNDERSLUNG NOSE INLET WITH VARIOUS  
NOSE CONFIGURATIONS AT MACH NUMBERS

FROM 1.55 TO 2.23\*

By Norman E. Sorensen and Rex R. Ellington

## SUMMARY

A wind-tunnel investigation was undertaken to evaluate some effects of inlet shape changes on the performance of an underslung nose inlet-duct combination. Two 2-shock and two 3-shock external compression inlets, and a 3-shock external-internal compression inlet were tested through a Mach number range of 1.55 to 2.23. Some of the 3-shock inlets were tested with boundary-layer control, with fences, and with a bypass system. Distortion of the total pressure over the engine compressor face, total-pressure recovery at the compressor, and external-chord-force coefficient were obtained throughout a large angle-of-attack and mass-flow-ratio range. Limited tests were made at an angle of sideslip.

The proper shaping of the compression surfaces and the inlet lips appears to be the most important problem in providing the best total-pressure recovery. The addition of full fences provided the best means for improving the total-pressure recovery by effectively reshaping the inlet lips instead of the compression surfaces. The 3-shock external-internal compression inlet provided the same or better total-pressure recovery at the higher Mach numbers without the use of fences.

## INTRODUCTION

Underslung nose inlets, such as described in reference 1, require the fuselage to function as an efficient compression surface while still meeting the usual requirements of a fuselage forebody. Careful consideration must therefore be given to the interrelationship between the shape of the fuselage and the shape of the inlet so that, among other requirements, the compression shock waves fall in the proper relationship to the lips of the inlet at the design Mach number.

\*Title, Unclassified

[REDACTED]

UNCLASSIFIED

In order to evaluate some effects of inlet and nose shape changes on the performance of an air induction system, a brief investigation of a model with an underslung nose inlet has been conducted. Various inlet compression surface and lip arrangements were investigated. Two 2-shock and two 3-shock external compression inlets, and a 3-shock external-internal compression inlet were tested. Some of the 3-shock inlets were tested with boundary-layer control, with fences, and with a bypass system.

The tests were conducted in the 9- by 7-foot test section of the Ames Unitary Plan wind tunnel. The range of Mach numbers was from 1.55 to 2.23, and the range of angles of attack was from about  $-5^\circ$  to  $+14^\circ$ . Limited tests were conducted at  $5^\circ$  or  $10^\circ$  angle of sideslip. The Reynolds number was about  $2.5 \times 10^6$  per foot.

#### SYMBOLS

$A_{BP}$	minimum bypass area (see fig. 2)
$A_m$	maximum body cross-sectional area (see fig. 3)
$A_1$	minimum inlet area (see fig. 3)
$C_X$	external-chord-force coefficient based on maximum body cross-sectional area
$M_\infty$	free-stream Mach number
$m_3$	mass rate of flow through the model engine compressor face
$m_\infty$	mass rate of flow of free-stream air through an area equal to $A_1$
$P_{t3}$	total pressure at the engine compressor face
$P_{t\infty}$	total pressure of the free stream
$\Delta p$	total pressure distortion parameter at the engine compressor face, $\frac{(P_{t3})_{\max} - (P_{t3})_{\min}}{(P_{t3})_{av}}$
$R$	free-stream Reynolds number per foot
$\alpha$	angle of attack measured from the body reference axis
$\beta$	angle of sideslip, positive to the left

CONFIDENTIAL

~~CONFIDENTIAL~~

### Subscript

crit    critical inlet condition (normal shock wave at the minimum inlet area)

Configuration notation:		Number of shocks
1	22.5°	2
2	25° nose	2
3	15°-25° nose	3
3F	15°-25° nose with fences	3
3F <sub>s</sub>	15°-25° nose with fences and area suction	3
3BPS	15°-25° nose with small bypass	3
3BPL	15°-25° nose with large bypass	3
4	15°-25° cone	3
4-1/2F	15°-25° cone with half fences	3
4F	15°-25° cone with full fences	3
5	scoop without bleed	3
5B	scoop with bleed slot	3
6	aerodynamic fairing	None

### MODEL DESCRIPTION

The model consisted of a fuselage forebody and the inlet. Figure 1 shows the model mounted on a sting in the wind tunnel. Figure 2 is a drawing of the model and its instrumentation. Details of the various configurations tested are shown in figure 3 together with the design Mach numbers, maximum body cross-sectional areas, and minimum inlet areas. Figure 4 shows detail photographs of the models. The duct area distributions up to the compressor rake station are presented in figure 5.

Details of the engine compressor face rake, the exit rake, and the bypass system are shown in figure 2. A small and a large bypass system were tested, the small having half the area of the large. The bypass

total-pressure rake was located at the minimum bypass cross-sectional area. Four static-pressure orifices were located in the base of the model, and three static-pressure orifices were located in the balance chamber housing. Mass flow through the duct was regulated by a movable plug at the base of the model. A static-pressure transducer was mounted in the duct to measure flow stability limits. A balance was housed within the engine compressor center body to measure the drag.

The various nose and inlet configurations are shown in figure 3. The noses and inlets differed not only in the obvious compression surface angles and arrangements but also in other less apparent aspects. The inlet shape of configuration 1 was nearly circular; the inlet shapes of configurations 2, 3 (all), and 4 (all) were identical and had a considerable amount of oblateness; the inlet shape of configuration 5 was even more oblate, to the extent that the bottom surface was nearly flat. The lower surface segments of the noses ahead of the inlets for configurations 1 and 2 were portions of single cones having half-angles of  $22.5^\circ$  and  $25^\circ$ , respectively; the conical portions were bounded by elements connecting the cone apex and the intersections of the inlet lips with the fuselage; above these elements the nose faired into the upper surface of the fuselage. Configuration 3 had a double conical nose designed in the same manner as configurations 1 and 2, that is, the conical surfaces were bounded by elements connecting the cone apex and the intersections of the inlet lips with the fuselage. The nose shapes of configurations 4, 4-1/2, and 5 were cones having angles as designated in figure 3; the conical shapes extended circumferentially to the extent necessary to insure that all inlet flow was generated from a true conical surface (this was in contrast to configurations 1, 2, and 3 in which inlet flow was influenced by the faired surface between the cone and the top of the fuselage); thus, the upper boundaries of the cones of configurations 4 and 5 were helical lines from the top of the fuselage to the intersections of the fuselage and inlet lips; the upper boundary of the cone of configuration 4-1/2 was a helical line to the intersections of the leading edges of the fences and the nose. Inasmuch as configuration 4F had full fences, the compression surfaces were simply true cones between the fences.

#### TEST METHODS

Total-pressure recovery and mass flow were obtained by the area weighted method using the rake at the engine compressor face. The external-chord-force coefficient  $C_x$  was computed by correcting the balance chord force for base pressure, for balance chamber pressure, and for internal-chord force. The  $C_x$  values for configurations 1, 2, and 3 were inaccurate because of defects in the exit rake and are not presented. When comparisons are made of  $C_x$  that are comparable, care should be exercised since the external aerodynamic shapes are not always similar or realistic.

In the cases where excess air was bypassed, the additional internal drag was taken into account. The bypass was on one side only and the mass flow through it was calculated from the total-pressure rake located at the minimum bypass area, with choked flow assumed at all times. Flow stability limits were obtained by observing the root mean square electrical output from the static-pressure transducer.

## RESULTS AND DISCUSSION

A summary of configurations tested and test conditions is given in table I. Table II presents the data for configurations 4 (all), 5 (all), and 6 which are not shown in the figures. Tabulated data for configurations 1, 2, and 3 (all) are not presented because they had inferior total-pressure recovery.

The quantities  $\Delta p$ ,  $p_{t3}/p_{t\infty}$ , and  $C_x$  for selected configurations are presented in figures 6 through 11. These figures are included in order to illustrate the general operating characteristics of the inlets, for example, stable range of operation, effect of crossflow, mass-flow variations, compressor face total-pressure distortion, etc.

The primary results of this investigation are summarized in figure 12. Figure 12 presents total-pressure recoveries throughout the Mach number range for the various inlet configurations when operating at critical mass-flow ratio. From comparisons of the results obtained for configurations 3 and 4, it is evident that configuration 3 had considerably lower pressure recovery at the design Mach number and above. The decrement in pressure recovery shown by configuration 3 illustrates the penalty that can be incurred if the proper shape of a compression surface is not maintained circumferentially to a sufficient extent. As a result of this design deficiency, compressed air is able to drain around the nose, away from the inlet, so that ingested air is not uniformly compressed and pressure recovery is adversely affected. Configuration 4, by virtue of its complete compression surface, provided uniformly compressed air and, consequently, higher pressure recoveries.

Inasmuch as an incomplete compression surface allows the compressed air to spill away from the inlet, fences offer a means of counteracting the effects of incomplete compression surfaces. It is evident from the results shown in figure 12 that partial fences, configuration 4-1/2F, are as effective as the complete compression surfaces of configuration 4. Moreover, full fences, configuration 4F, offer performance substantially better than that of either partial fences or complete compression surfaces.

The scoop inlet, configuration 5B, had pressure recovery characteristics that compared very favorably with the best of the other configurations shown in figure 12. This inlet is not directly comparable with

the other inlets, since it is of a somewhat different type and also was designed for a higher Mach number. It does indicate, however, the possibilities of an alternate design that avoids the use of fences.

#### CONCLUDING REMARKS

From the results of an investigation of underslung scoop inlet configurations some general statements can be made that apply to the configurations tested: The proper shaping of the compression surfaces and the inlet lips appears to be the most important problem in providing the best total-pressure recovery. The addition of full fences appears to provide a means for improving the total-pressure recovery by effectively reshaping the inlet lips instead of the compression surfaces. The scoop provides the same or better total-pressure recovery at the higher Mach numbers without the use of fences.

Ames Research Center  
National Aeronautics and Space Administration  
Moffett Field, Calif., Feb. 18, 1959

#### REFERENCES

1. Pfyl, Frank A.: An Investigation of the Effects of Nose and Lip Shapes for an Underslung Scoop Inlet at Mach Numbers From 0 to 1.9. NACA RM A55G13, 1955.
2. Davis, Wallace F., and Scherrer, Richard: Aerodynamic Principles for the Design of Jet-Engine Induction Systems. NACA RM A55F16, 1956.

TABLE I.- A SUMMARY OF CONFIGURATIONS AND TEST CONDITIONS

Figure (1)	Configuration	Configuration number	Mach number	Angle of attack, deg	Angle of sideslip, deg
6	22.5° nose	1	1.55, 1.70, 1.90	-3.0 to 13.5	0.1, 4.9
7	25° nose	2	1.70, 1.90, 2.23	-3.0 to 13.7	0.1, 4.9
8	15°-25° nose	3	1.55, 1.70, 1.90 2.10, 2.20	-2.2 to 13.6	0.1, 4.9
	15°-25° nose plus fences	3F	1.55, 1.70, 1.90 2.10, 2.20	-0.1 to 4.7	0.1, 4.9, 9.9
	15°-25° nose plus fences plus suction	3Fs	1.90, 2.06, 2.20	-0.1 to 4.6	0.1
None	15°-25° nose plus small bypass	3BPS	1.90, 2.20	4.3 to 4.7	-5.1, 0.1, 4.9
	15°-25° nose plus large bypass	3BPL	1.90, 2.20	4.3 to 4.7	-5.1, 0.1, 4.9
9	15°-25° cone	4	1.55, 1.90, 2.20	-2.7 to 8.6	0.1
	15°-25° cone plus half fences	4-1/2F	1.55, 1.90, 2.20	-2.7 to 8.8	0.1
	15°-25° cone plus full fences	4F	1.55, 1.90, 2.20	-2.7 to 8.6	0.1, 5.1, 10.1
None	Scoop	5	2.20	-0.3 to 4.7	0.1
10	Scoop plus bleed	5B	1.55, 1.70, 1.90 2.10, 2.20	-6.0 to 8.8	0.1, 5.1
None	Aerodynamic fairing	6	1.55, 1.70, 1.90	-3.0 to 13.5	-0.1, 0, 4.9

<sup>1</sup>The figures present typical data for one angle of attack only for each of the selected configurations.



TABLE II.- EXPERIMENTAL RESULTS

(a) Configuration 4.

$\Delta p$	$p_{t3}/p_{t\infty}$	$C_X$	$m_3/m_\infty$	$\Delta p$	$p_{t3}/p_{t\infty}$	$C_X$	$m_3/m_\infty$
$\alpha = -2.5; M_\infty = 1.56; \beta = 0.1$				$\alpha = -2.7; M_\infty = 1.90; \beta = 0.1$			
0.217	0.93	0.220	1.21	0.251	0.83	0.261	1.40
.210	.93	.265	1.21	.257	.83	.240	1.41
.209	.93	.245	1.21	.252	.83	.224	1.41
.208	.93	.242	1.21	.144	.86	.222	1.40
.178	.94	.239	1.19	.181	.88	.226	1.31
.139	.95	.249	1.08	.141	.89	.244	1.19
.105	.96	.272	.94	.064	.87	.277	1.03
.075	.96	.289	.83	.022	.84	.303	.81
.031	.96	.330	.62	.013	.82	.314	.68
.014	.96	.352	.47				
$\alpha = 4.6; M_\infty = 1.56; \beta = 0.1$				$\alpha = 8.3; M_\infty = 1.90; \beta = 0.1$			
0.212	0.93	0.277	1.21	0.259	0.85	0.277	1.44
.216	.93	.267	1.21	.266	.85	.268	1.44
.219	.93	.262	1.21	.263	.85	.254	1.43
.191	.94	.259	1.19	.299	.86	.252	1.40
.182	.94	.263	1.18	.223	.86	.267	1.29
.185	.94	.259	1.19	.161	.86	.268	1.19
.193	.94	.259	1.19	.064	.85	.302	1.02
.188	.94	.260	1.19	.022	.84	.339	.81
.140	.95	.267	1.08	-	.83	.374	.65
.105	.96	.278	.97				
.080	.96	.291	.85				
.047	.97	.331	.64				
.022	.97	.376	.45				
$\alpha = 8.6; M_\infty = 1.56; \beta = 0.1$				$\alpha = 4.7; M_\infty = 2.20; \beta = 0.1$			
0.222	0.91	0.293	1.19	0.248	0.72	0.265	1.58
.222	.92	.283	1.19	.248	.72	.244	1.58
.226	.91	.280	1.19	.251	.72	.278	1.58
.181	.93	.277	1.18	.240	.72	.256	1.58
.137	.95	.285	1.08	.235	.72	.226	1.59
.109	.96	.302	.96	.170	.74	.219	1.58
.081	.96	.319	.82	.233	.76	.217	1.52
.028	.96	.343	.65	.109	.75	.246	1.36
.018	.95	.378	.47	.041	.74	.261	1.23
.221	.92	.309	1.19	.021	.73	.289	1.07
.225	.91	.301	1.19	.001	.72	.341	.86

TABLE II.- EXPERIMENTAL RESULTS - Continued

(b) Configuration 4-1/2F

$\Delta p$	$P_{t3}/P_{t\infty}$	$C_X$	$m_3/m_\infty$	$\Delta p$	$P_{t3}/P_{t\infty}$	$C_X$	$m_3/m_\infty$
$\alpha = -2.4; M_\infty = 1.55; \beta = 0.1$				$\alpha = -2.7; M_\infty = 1.90; \beta = 0.1$			
-	0.92	0.369	0.35	0.252	0.82	0.227	1.38
0.020	.93	.334	.49	.156	.86	.209	1.37
.021	.93	.319	.54	.208	.87	.214	1.32
.039	.94	.308	.65	.147	.88	.239	1.16
.068	.95	.291	.81	.073	.88	.273	.99
.089	.95	.271	.88	.044	.87	.296	.86
.098	.95	.274	.93	.042	.83	.300	.82
.124	.95	.271	1.02	$\alpha = 8.8; M_\infty = 1.90; \beta = 0.1$			
.148	.94	.258	1.08	0.308	0.85	0.259	1.42
.173	.94	.263	1.14	.293	.85	.235	1.42
.200	.93	.269	1.18	.297	.85	.215	1.42
.208	.93	.243	1.20	.293	.85	.257	1.42
.214	.93	.364	1.20	.296	.85	.209	1.42
$\alpha = 4.6; M_\infty = 1.55; \beta = 0.1$				.314	.85	.158	1.41
0.015	0.96	0.392	0.28	.299	.85	.192	1.39
.025	.96	.344	.46	.268	.85	.192	1.34
.050	.96	.339	.52	.174	.84	.213	1.23
.059	.96	.301	.69	.125	.84	.248	1.15
.080	.96	.293	.76	.089	.84	.241	1.08
.164	.95	.304	.88	.033	.83	.316	.77
.204	.93	.310	1.12	.034	.83	.301	.79
.208	.92	.286	1.18	.029	.83	.303	.77
.210	.92	.273	1.18	.039	.83	.309	.71
.211	.92	.270	1.19	.027	.83	.350	.58
.038	.92	.282	1.19	.011	.83	.359	.52
$\alpha = 9.1; M_\infty = 1.55; \beta = 0.1$				$\alpha = 4.7; M_\infty = 2.20; \beta = 0.1$			
0.040	0.94	0.287	0.55	0.253	0.75	0.268	1.63
.042	.95	.331	.51	.251	.75	.260	1.63
.104	.95	.319	.67	.211	.76	.204	1.63
.128	.94	.290	.88	.215	.76	.220	1.64
.220	.94	.295	1.01	.276	.77	.215	1.56
.239	.92	.269	1.15	.136	.75	.231	1.41
.234	.91	.314	1.17	.055	.74	.264	1.20
.237	.91	.290	1.18	.037	.73	.298	.99
.241	.90	.294	1.18	.012	.73	.337	.78
.295	.91	.289	1.18				

TABLE II.- EXPERIMENTAL RESULTS - Continued

(c) Configuration 4F

$\Delta p$	$P_{t3}/P_{t\infty}$	$C_X$	$m_3/m_\infty$	$\Delta p$	$P_{t3}/P_{t\infty}$	$C_X$	$m_3/m_\infty$
$\alpha = -2.4; M_\infty = 1.55; \beta = 0.1$				$\alpha = -2.7; M_\infty = 1.90; \beta = 0.1$			
0.216	0.93	0.287	1.20	0.248	0.82	0.268	1.37
.211	.93	.267	1.20	.241	.82	.250	1.37
.216	.93	.264	1.20	.255	.82	.226	1.37
.184	.94	.253	1.19	.195	.83	.218	1.37
.151	.95	.258	1.09	.197	.87	.220	1.30
.100	.95	.285	.94	.142	.87	.238	1.17
.071	.96	.297	.85	.104	.81	.268	1.04
.053	.93	.330	.70	.090	.79	.302	1.03
.040	.91	.360	.69	$\alpha = 4.3; M_\infty = 1.90; \beta = 5.1$			
$\alpha = 4.5; M_\infty = 1.56; \beta = 0.1$				0.228	0.90	0.283	1.49
0.216	0.93	0.290	1.21	.220	.90	.261	1.49
.225	.93	.265	1.21	.227	.90	.258	1.49
.220	.93	.265	1.21	.193	.92	.246	1.49
.188	.94	.254	1.19	.173	.91	.263	1.35
.138	.96	.262	1.09	.129	.91	.279	1.20
.097	.97	.276	.97	.063	.90	.301	1.05
.072	.97	.294	.85	.035	.86	.334	.87
.038	.98	.337	.62	.038	.87	.359	.89
.020	.96	.373	.47	$\alpha = 8.3; M_\infty = 1.90; \beta = 0.1$			
.221	.93	.276	1.21	0.224	0.90	0.269	1.50
.220	.93	.266	1.21	.221	.90	.257	1.50
$\alpha = 8.6; M_\infty = 1.56; \beta = 0.1$				.296	.90	.247	1.51
0.220	0.92	0.278	1.20	.193	.91	.245	1.48
.221	.93	.268	1.20	.155	.91	.262	1.33
.220	.93	.267	1.20	.088	.90	.267	1.20
.197	.94	.263	1.18	.042	.90	.295	1.05
.137	.96	.273	1.08	.029	.89	.337	.82
.102	.96	.288	.95	.022	.86	.373	.67
.080	.97	.299	.84	$\alpha = 4.7; M_\infty = 2.20; \beta = 0.1$			
.022	.97	.337	.62	0.243	0.78	0.257	1.70
.016	.97	.374	.42	.240	.78	.179	1.69
.220	.93	.275	1.20	.226	.78	.216	1.69
.218	.93	.276	1.20	.158	.80	.202	1.70
				.127	.81	.219	1.59
				.066	.80	.246	1.42
				.037	.78	.271	1.24
				.079	.75	.312	1.19

TABLE II.- EXPERIMENTAL RESULTS - Continued

(d) Configuration 5

$\Delta p$	$p_{t3}/p_{t\infty}$	$C_X$	$m_3/m_\infty$
$\alpha = -0.3; M_\infty = 2.20; \beta = 0.1$			
0.315	0.72	0.295	1.58
.207	.78	.212	1.62
.132	.81	.247	1.52
.133	.80	.266	1.42
.067	.81	.306	1.18
.014	.78	.382	.90
.017	.78	.385	.89
.115	.80	.259	1.41
.092	.81	.278	1.24
$\alpha = 4.7; M_\infty = 2.20; \beta = 0.1$			
0.315	0.73	0.314	1.59
.226	.79	.175	1.64
.100	.82	.256	1.52
.107	.81	.277	1.43
.071	.78	.301	1.21
.022	.74	.366	.88

TABLE II.- EXPERIMENTAL RESULTS - Continued

(e) Configuration 5B

$\Delta p$	$P_{t3}/P_{t\infty}$	$C_X$	$m_3/m_\infty$	$\Delta p$	$P_{t3}/P_{t\infty}$	$C_X$	$m_3/m_\infty$	$\Delta p$	$P_{t3}/P_{t\infty}$	$C_X$	$m_3/m_\infty$
$\alpha = -5.5; M_\infty = 1.55; \beta = 0.1$				$\alpha = -3.7; M_\infty = 1.90; \beta = 0.1$				$\alpha = 8.8; M_\infty = 2.10; \beta = 0.1$			
0.158	0.89	0.119	1.08	0.213	0.77	0.289	1.31	0.340	0.76	0.317	1.54
.129	.93	.264	1.04	.216	.77	.171	1.31	.334	.76	.268	1.54
.109	.94	.264	.96	.157	.85	.223	1.28	.310	.76	.256	1.54
.079	.96	.293	.77	.142	.88	.291	1.01	.273	.78	.248	1.56
.032	.98	.362	.50	.046	.89	.314	.83	.160	.85	.250	1.54
.014	.98	.382	.39	.027	.86	.361	.71	.105	.83	.281	1.39
.0215	.83	.294	1.08	$\alpha = 4.3; M_\infty = 1.90; \beta = 0.1$				.099	.81	.303	1.24
$\alpha = 4.6; M_\infty = 1.55; \beta = 0.1$				0.239	0.81	0.302	1.37	.041	.79	.338	1.01
0.192	0.85	0.303	1.11	.241	.81	.275	1.37	.017	.76	.400	.74
.201	.85	.261	1.11	.149	.90	.250	1.34	-	.76	.410	.71
.154	.93	.260	1.07	.105	.90	.302	1.06	$\alpha = -3.3; M_\infty = 2.20; \beta = 0.1$			
.081	.96	.296	.84	.064	.92	.356	.83	0.374	0.70	0.290	1.56
.040	.97	.332	.64	.015	.94	.435	.55	.369	.70	.227	1.57
.029	.97	.372	.48	.126	.89	.300	1.13	.374	.70	.217	1.57
$\alpha = 8.6; M_\infty = 1.55; \beta = 0.1$				$\alpha = 8.3; M_\infty = 1.90; \beta = 0.1$				.333	.73	.225	1.59
0.192	0.85	0.324	1.11	0.237	0.81	0.338	1.37	.132	.80	.224	1.58
.198	.85	.279	1.11	.244	.81	.269	1.37	-	.82	.239	1.45
.143	.94	.277	1.07	.188	.90	.241	1.36	.156	.79	.263	1.30
.135	.94	.296	1.05	.114	.91	.270	1.24	.119	.78	.285	1.20
.075	.97	.305	.86	.110	.90	.302	1.08	.047	.77	.316	1.08
.046	.98	.349	.63	.061	.89	.353	.84	$\alpha = 4.7; M_\infty = 2.20; \beta = 0.1$			
.021	.98	.395	.44	.021	.87	.391	.68	0.382	0.72	0.367	1.60
$\alpha = -6.0; M_\infty = 1.70; \beta = 0.1$				$\alpha = -3.3; M_\infty = 2.10; \beta = 0.1$				.388	.72	.262	1.61
0.219	0.80	0.301	1.15	0.308	0.75	0.296	1.51	.391	.72	.224	1.61
.206	.80	.249	1.16	.303	.75	.239	1.51	.330	.75	.239	1.63
.147	.89	.253	1.15	.314	.75	.233	1.51	.137	.82	.242	1.61
.107	.92	.286	.91	.276	.77	.225	1.53	.091	.81	.249	1.49
.045	.96	.341	.68	.170	.84	.228	1.51	.095	.79	.279	1.36
.022	.93	.371	.54	.116	.84	.259	1.34	.056	.77	.305	1.16
$\alpha = 4.0; M_\infty = 1.70; \beta = 0.1$				.151	.83	.255	1.25	.030	.74	.340	.95
0.195	0.82	0.325	1.18	.039	.82	.311	.97	$\alpha = 8.7; M_\infty = 2.20; \beta = 0.1$			
.213	.82	.326	1.19	.034	.80	.350	.94	0.355	0.71	0.329	1.57
.202	.82	.269	1.19	$\alpha = 4.8; M_\infty = 2.10; \beta = 0.1$				.366	.71	.260	1.58
.154	.91	.261	1.16	0.320	0.76	0.305	1.54	.356	.71	.268	1.58
.087	.94	.303	.90	.310	.76	.261	1.54	.316	.73	.233	1.60
.055	.95	.349	.68	.312	.77	.240	1.55	.138	.80	.230	1.59
.034	.95	.389	.52	.273	.79	.235	1.57	.089	.77	.276	1.43
$\alpha = 8.0; M_\infty = 1.70; \beta = 0.1$				.169	.86	.250	1.54	.093	.76	.281	1.32
0.206	0.83	0.309	1.21	.094	.87	.270	1.39	.065	.75	.289	1.20
.204	.83	.281	1.21	.123	.84	.303	1.24	.024	.72	.360	.89
.153	.92	.271	1.17	.042	.81	.338	1.00				
.087	.94	.307	.93	.017	.79	.380	.80				
.053	.95	.358	.69								
.045	.95	.373	.63								
.029	.95	.402	.49								

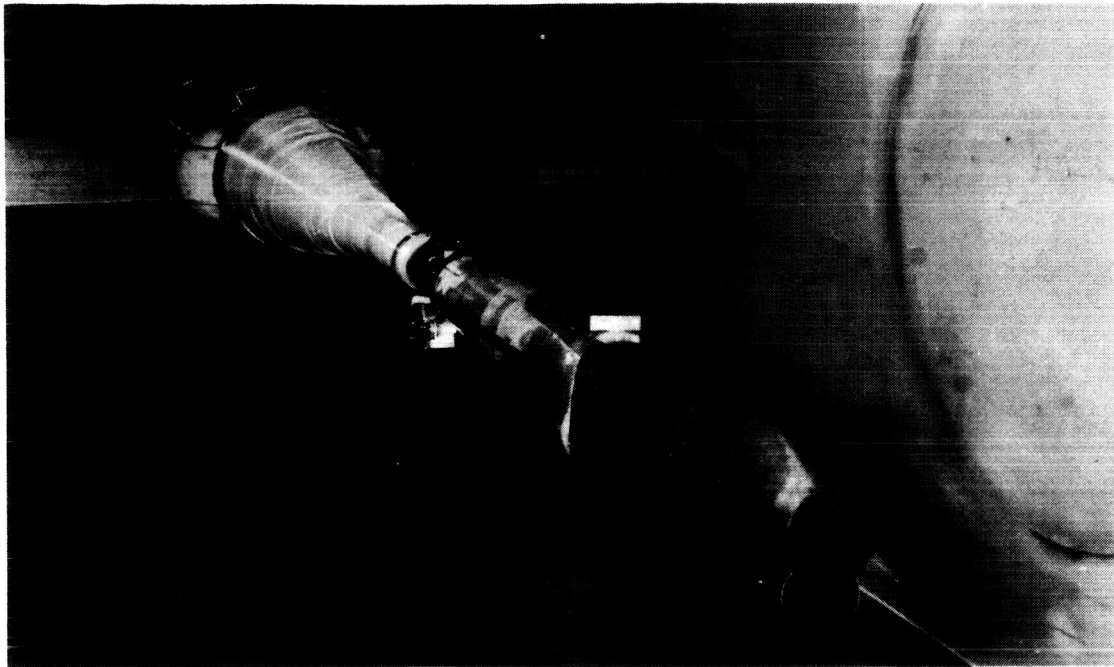
TABLE II.- EXPERIMENTAL RESULTS - Concluded

(f) Configuration 6

$M_\infty$	$\alpha$	$\beta$	$C_X$
1.56	-2.5	0	0.165
	-2.5	0	.171
	4.5	0	.135
	9.5	0	.122
	13.5	0	.115
1.70	13.0	-0.1	0.086
	9.0	-.1	.102
	4.0	-.1	.120
	4.0	4.9	.133
	-3.0	-.1	.175
	-3.0	-.1	.175
1.90	-2.7	-0.1	0.167
	4.3	-.1	.130
	9.3	-.1	.105
	13.3	-.1	.086

~~CONFIDENTIAL~~

~~CONFIDENTIAL~~



A-21820

Figure 1.- A typical configuration mounted in the wind tunnel.



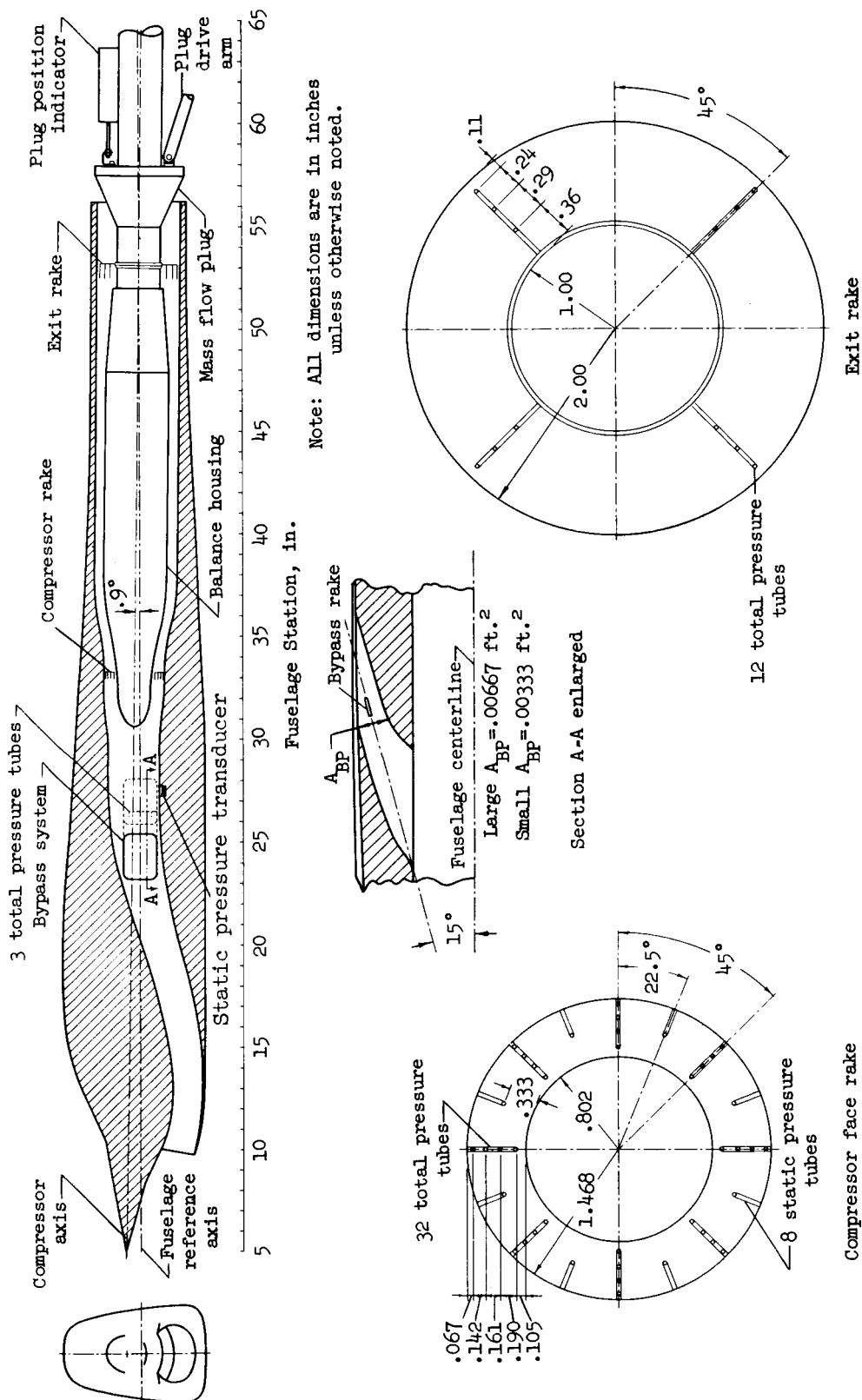
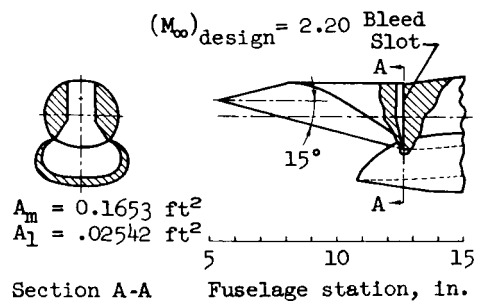
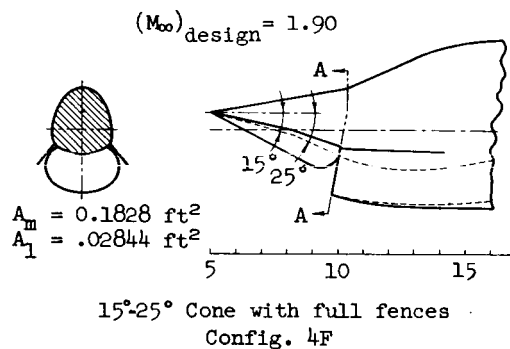
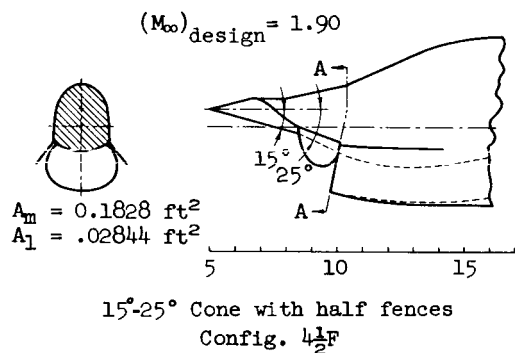
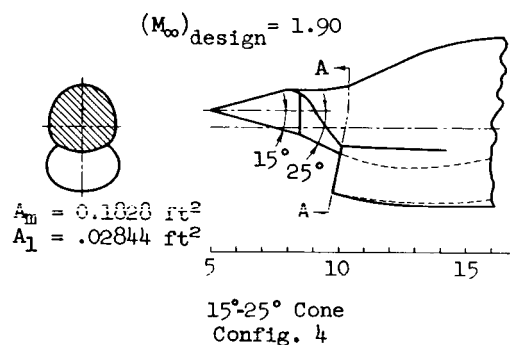
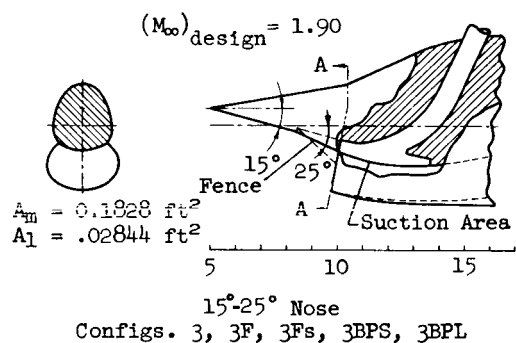
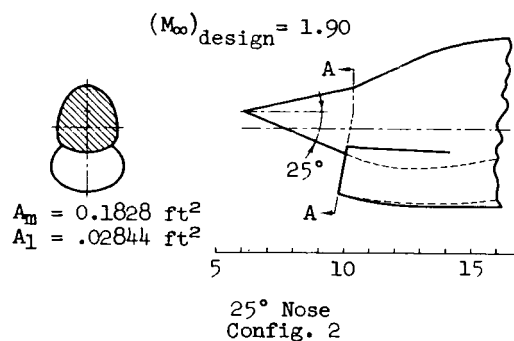
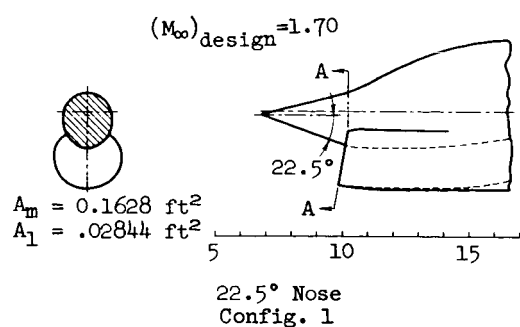
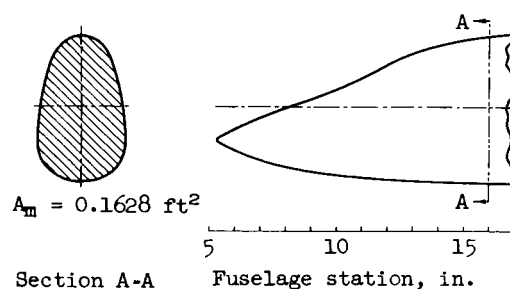


Figure 2.- Drawing of the model and details of the instrumentation.



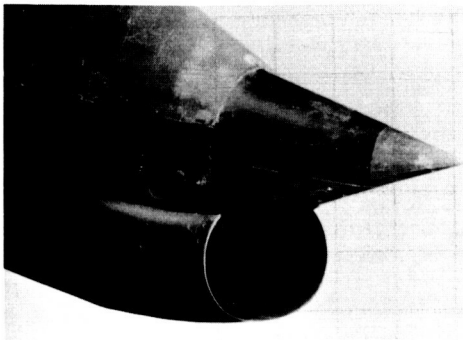
Scoop  
 Configs. 5, 5B



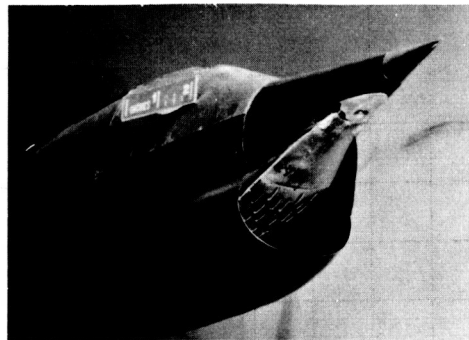
Aerodynamic Fairing  
 Config. 6

Figure 3.- Details of the various nose configurations.

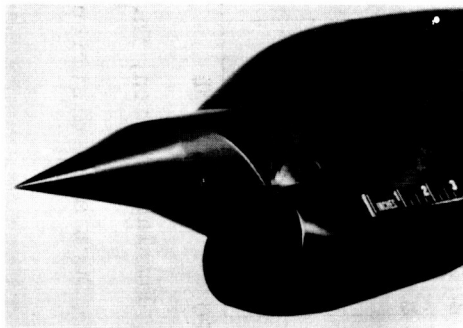
SECRET



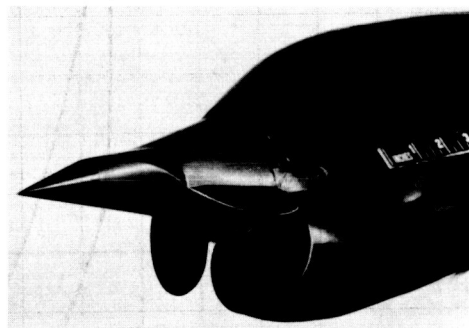
25° nose, configuration 2.



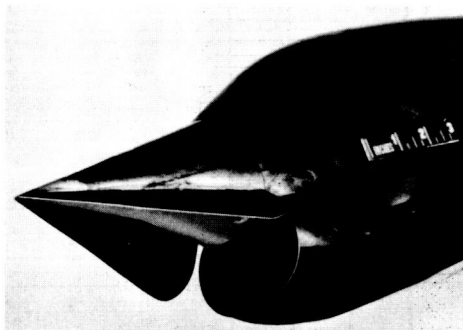
15°-25° nose with fences and suction, configuration 3Fs.



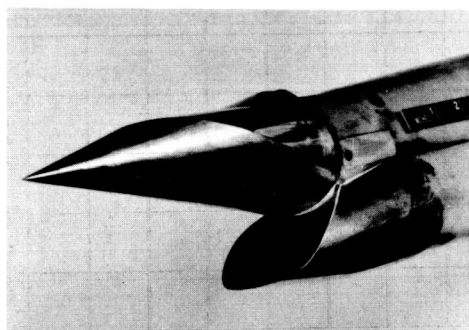
15°-25° cone with half fences, configuration 4-1/2 F.



15°-25° cone, configuration 4.



15°-25° cone with full fences, configuration 4F.



Scoop, configuration 5B.

A-24515

Figure 4.- Photographs of the various nose inlet configurations.

SECRET

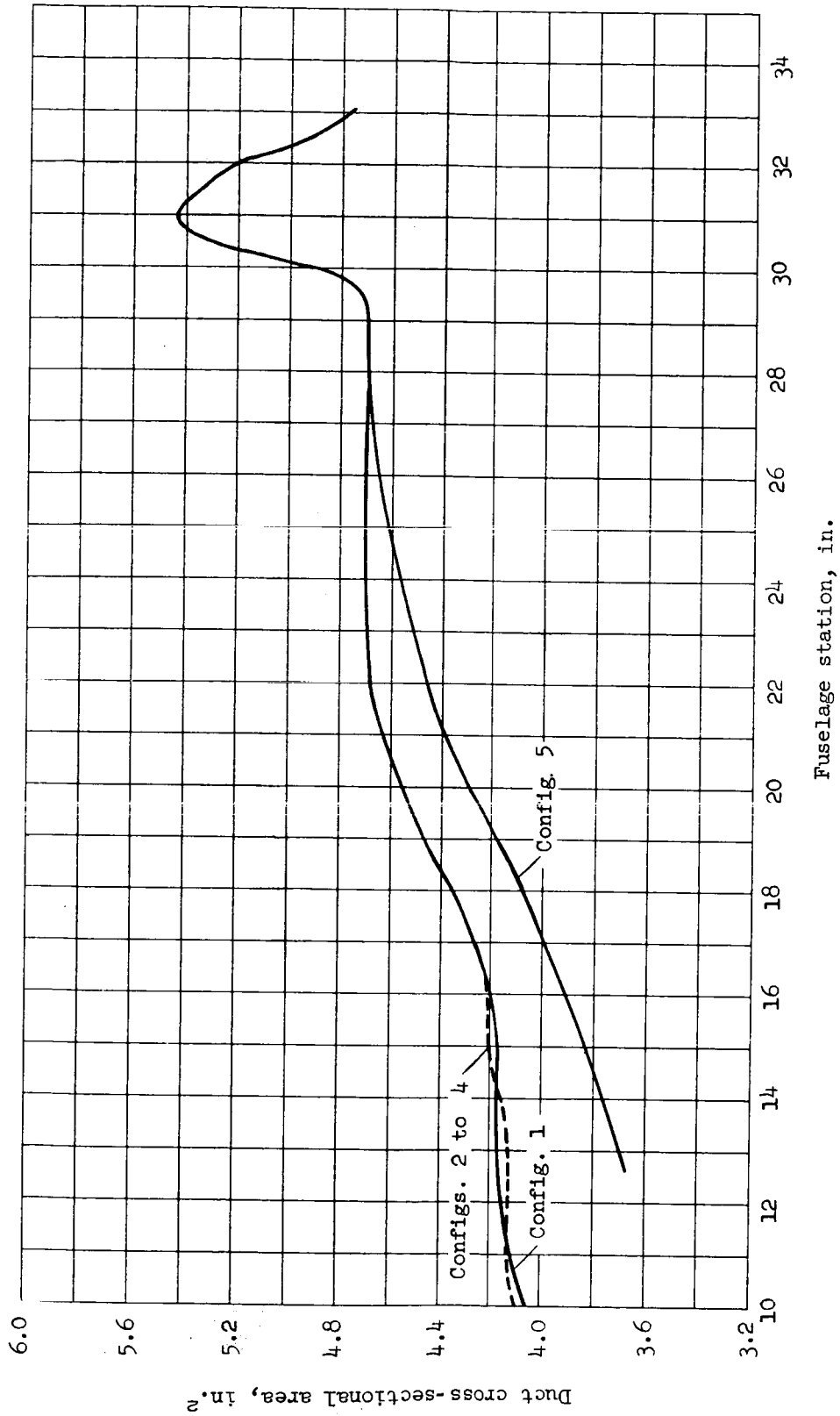


Figure 5.- Duct area distributions.

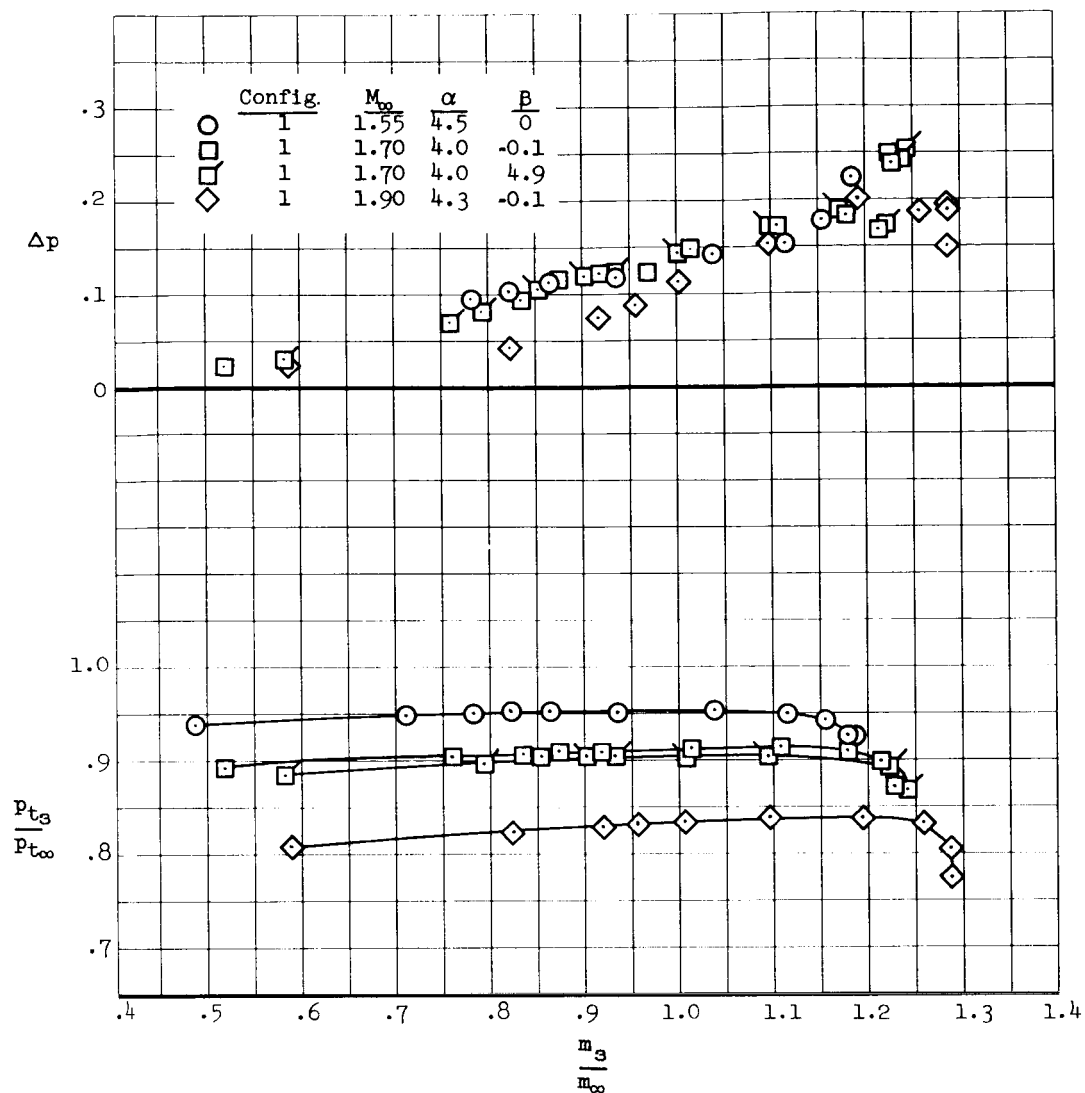


Figure 6.- Performance characteristics for the 22.5° nose inlet at nearly constant angle of attack and variable Mach number.

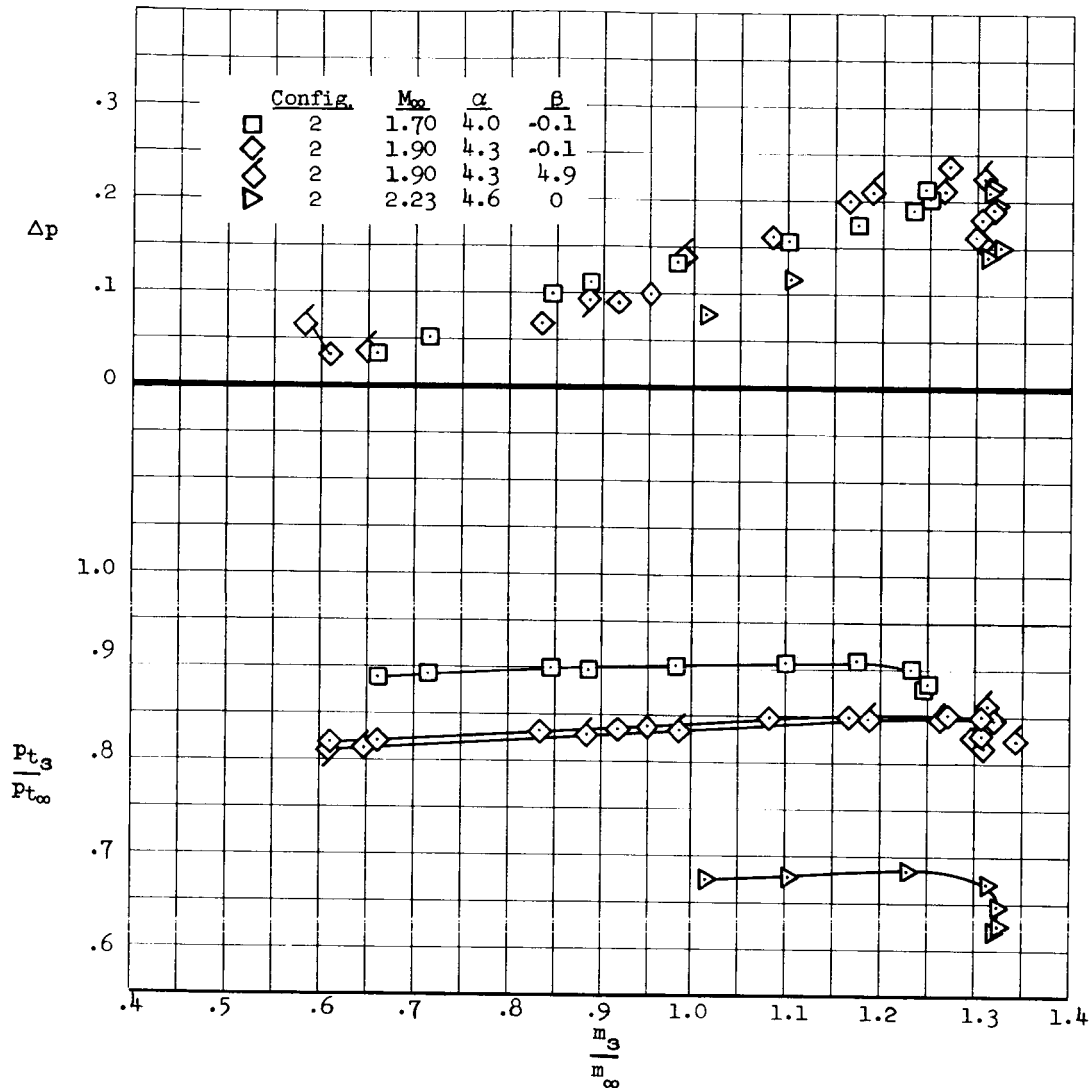


Figure 7.- Performance characteristics for the 25° nose inlet at nearly constant angle of attack and variable Mach number.

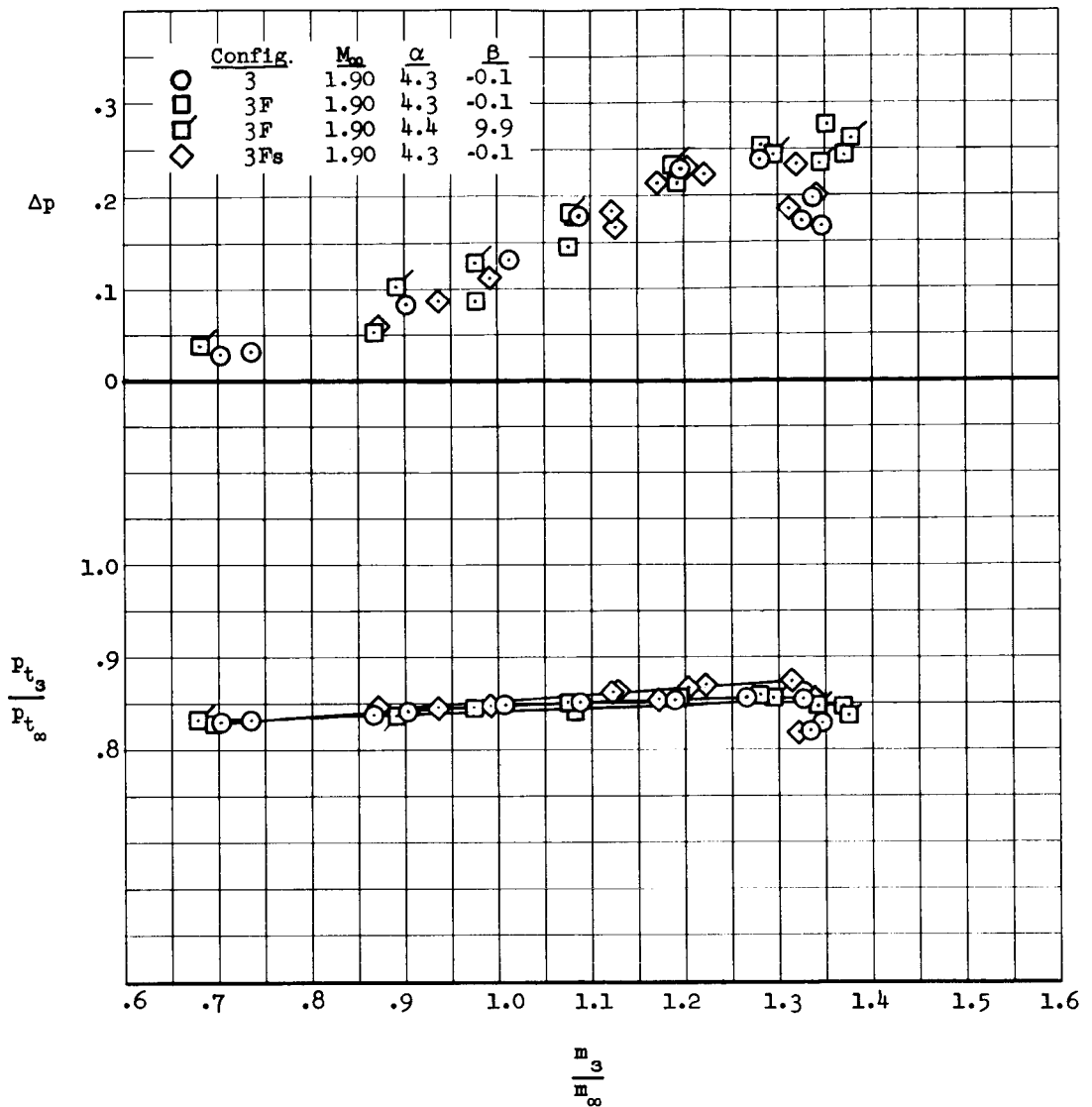


Figure 8.- Performance characteristics for the 15°-25° nose inlet with fences and fences and suction at a constant angle of attack.

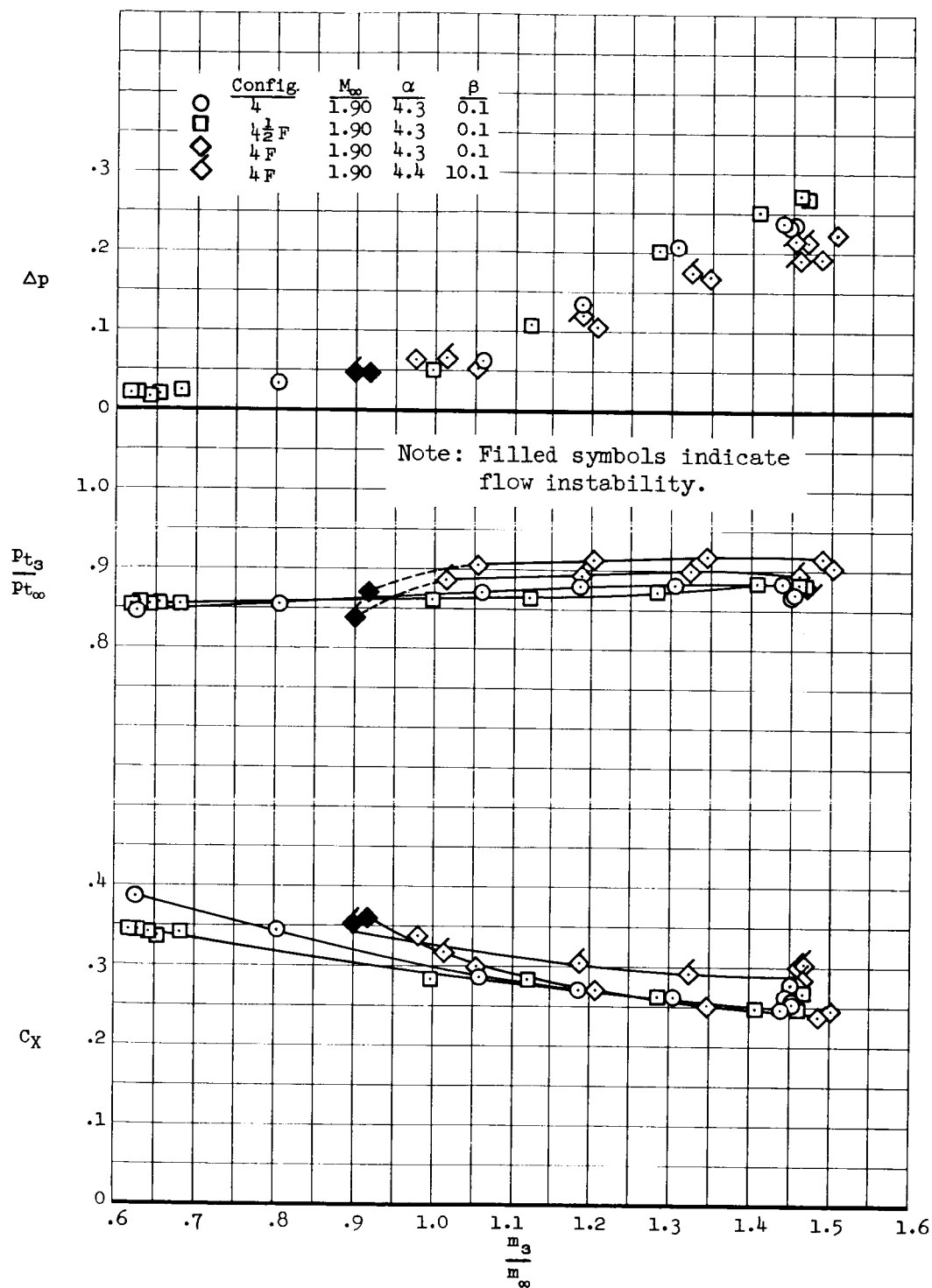


Figure 9.- Performance characteristics for the 15°-25° cone inlet with half and full fences at a constant angle of attack and Mach number.



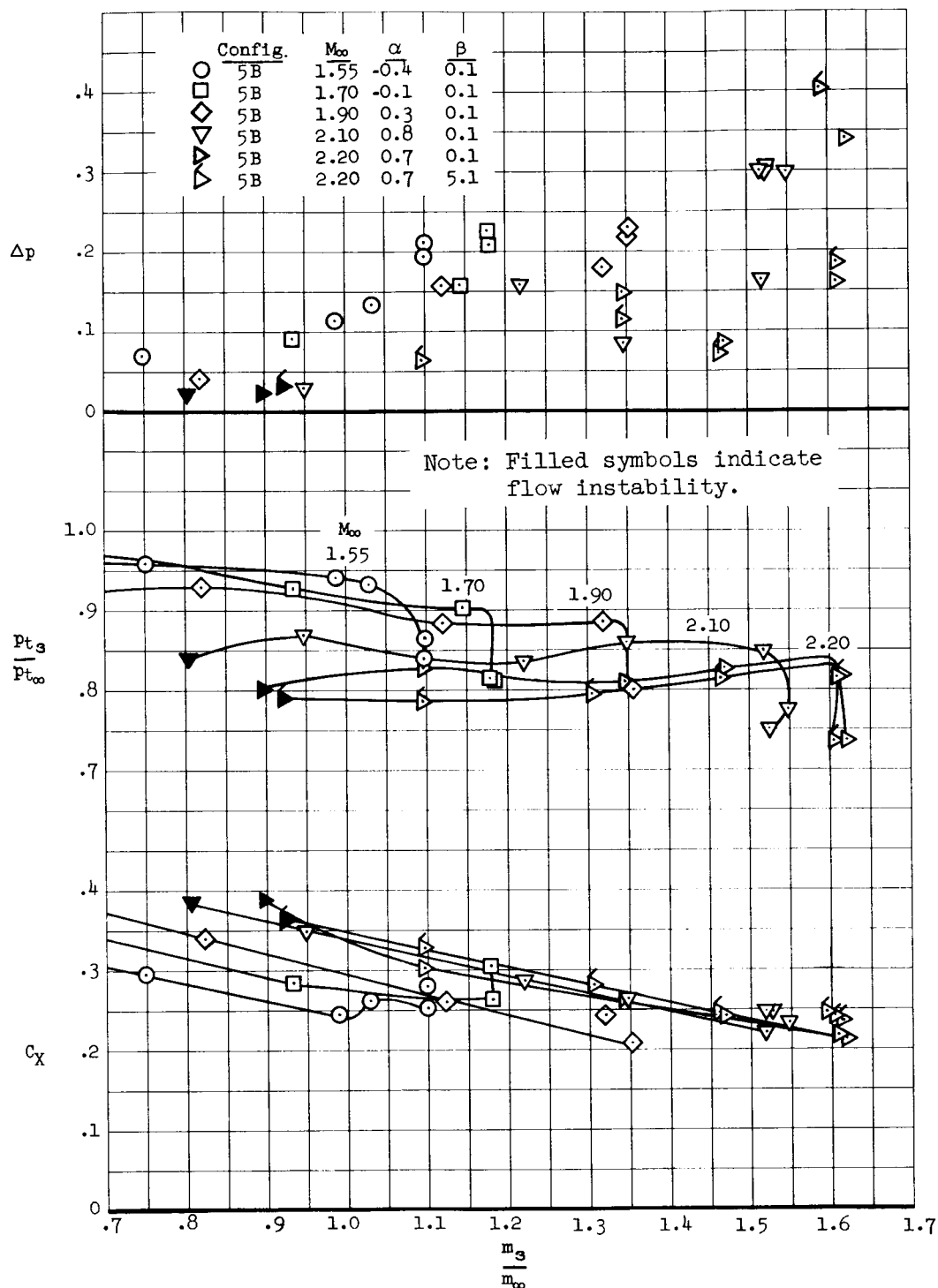
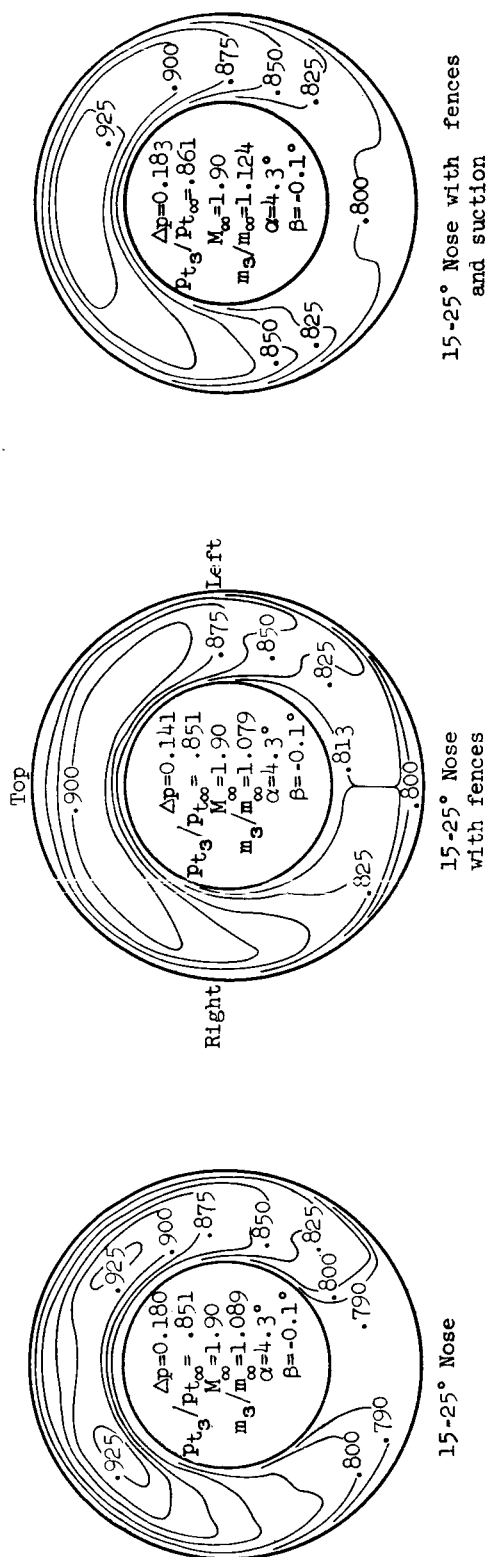


Figure 10.- Performance characteristics for the scoop at a nominally constant angle of attack and variable Mach number.



Front views looking into the compressor

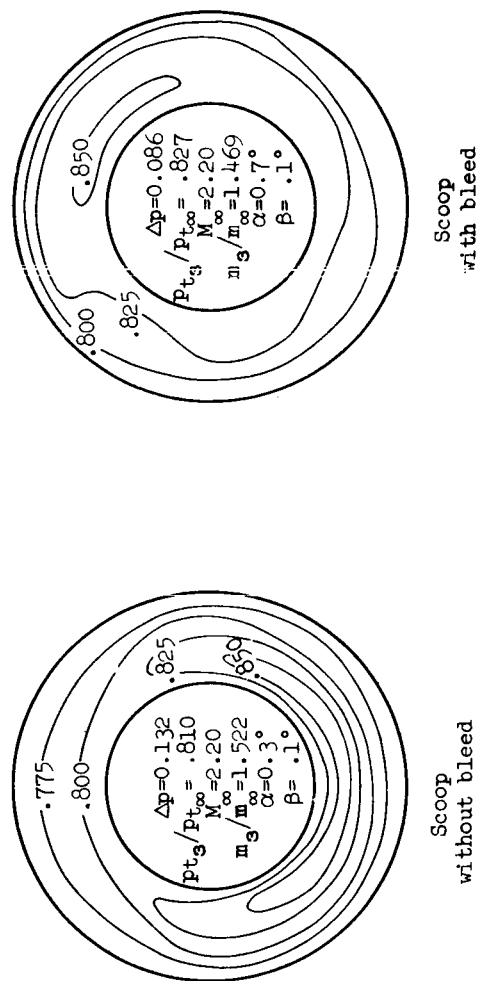


Figure 11.- Typical contour plots of the local total-pressure recovery at the engine compressor face for several configurations.

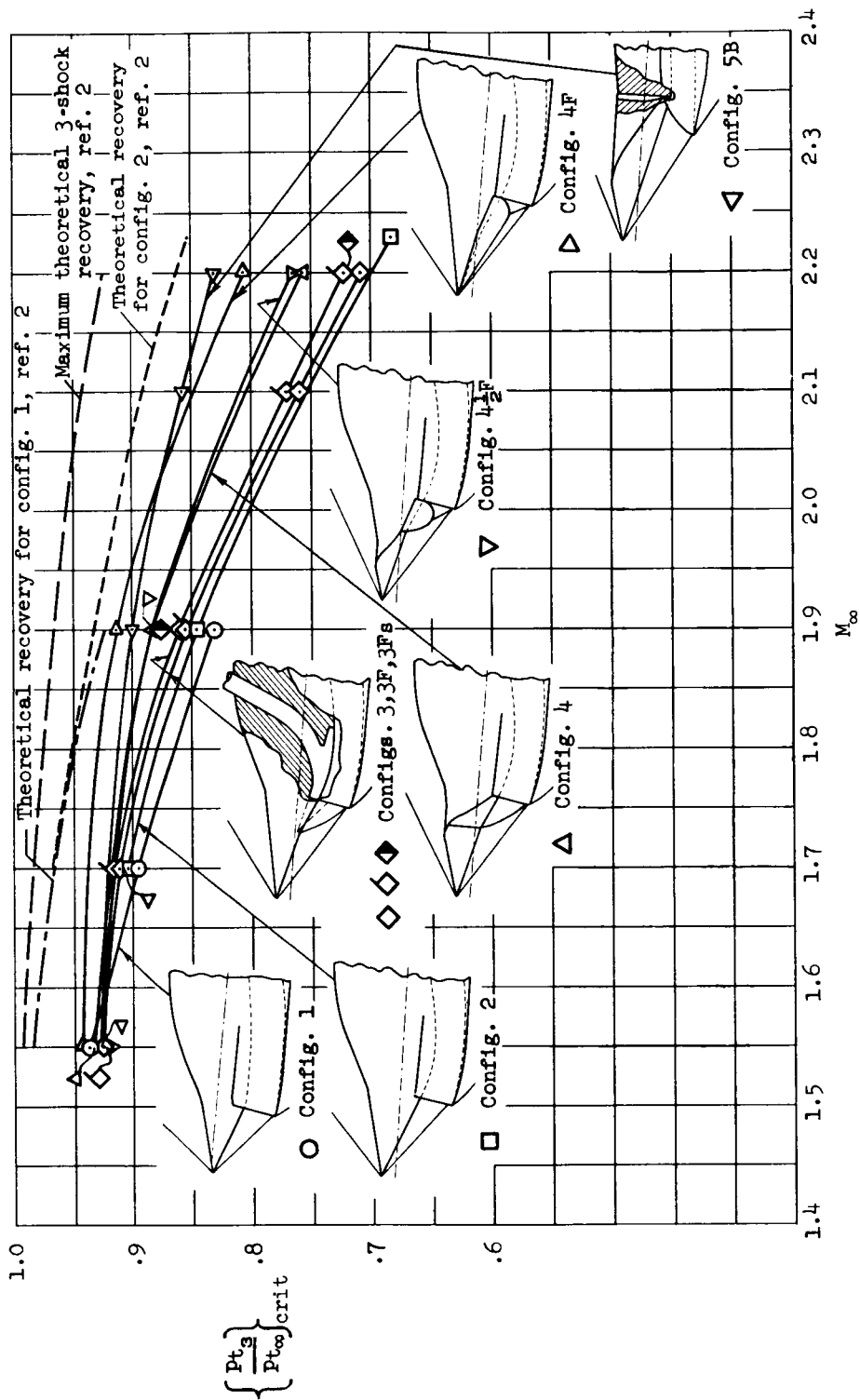

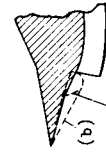

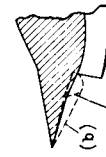

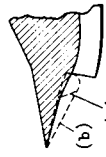

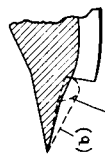


Figure 12.- Variation of total-pressure recovery and external-chord-force coefficient with free-stream Mach number at critical mass-flow ratio for the various nose inlet configurations.

NOTES: (1) Reynolds number is based on the diameter of a circle with the same area as that of the capture area of the inlet.

(2) The symbol \* denotes the occurrence of buzz.

Report and facility	Description				Test parameters					Test data				Performance		Remarks
	Configuration	Number of oblique shocks	Type of boundary-layer control	Free-stream Mach number	Reynolds number $\times 10^{-6}$	Angle of attack, deg	Angle of yaw, deg	Drag	Inlet-flow profile	Discharge-flow profile	Flow picture	Maximum total-pressure recovery	Mass-flow ratio			
NASA TM X-14 Ames 9- by 7- Foot Wind Tunnel			2	None	1.90	.39	4.3	0.1	✓			0.884	.626 - 1.453	No fences		
				None	1.90	.39	4.3	.1	✓			.884	.620 - 1.468	Fences (a)		
				None	1.90	.39	4.3	.1	✓			.918	.917 - 1.502*	Fences (b)		
				Throat slot	2.20	.45	.7	.1	✓			.830	.895 - 1.620*	Scoop type inlet		
NASA TM X-14 Ames 9- by 7- Foot Wind Tunnel			2	None	1.90	.39	4.3	0.1	✓			0.884	.626 - 1.453	No fences		
				None	1.90	.39	4.3	.1	✓			.884	.620 - 1.468	Fences (a)		
				None	1.90	.39	4.3	.1	✓			.918	.917 - 1.502*	Fences (b)		
				Throat slot	2.20	.45	.7	.1	✓			.830	.895 - 1.620*	Scoop type inlet		
NASA TM X-14 Ames 9- by 7- Foot Wind Tunnel			2	None	1.90	.39	4.3	0.1	✓			0.884	.626 - 1.453	No fences		
				None	1.90	.39	4.3	.1	✓			.884	.620 - 1.468	Fences (a)		
				None	1.90	.39	4.3	.1	✓			.918	.917 - 1.502*	Fences (b)		
				Throat slot	2.20	.45	.7	.1	✓			.830	.895 - 1.620*	Scoop type inlet		
NASA TM X-14 Ames 9- by 7- Foot Wind Tunnel			2	None	1.90	.39	4.3	0.1	✓			0.884	.626 - 1.453	No fences		
				None	1.90	.39	4.3	.1	✓			.884	.620 - 1.468	Fences (a)		
				None	1.90	.39	4.3	.1	✓			.918	.917 - 1.502*	Fences (b)		
				Throat slot	2.20	.45	.7	.1	✓			.830	.895 - 1.620*	Scoop type inlet		

#### Bibliography

These strips are provided for the convenience of the reader and can be removed from this report to compile a bibliography of NASA inlet reports. This page is being added only to inlet reports and is on a trial basis.